**Proceedings of the ASME 2016 Dynamic Systems and Control Conference**
**DSCC2016**
**October 12-14, 2016, Minneapolis, Minnesota, USA**

**DSCC2016-9699**

# ON-LINE ESTIMATION OF WHEELCHAIR TIRE SLIP UTILIZING AN INSTANTANEOUS CENTER OF ROTATION EXTENDED KALMAN FILTER

**Kelilah Wolkowicz**[1]* **Jesse Pentzer**[2] **Christopher Miller**[3] **Jason Z. Moore**[1] **Sean N. Brennan**[1]

[1]Mechanical and Nuclear Engineering
The Pennsylvania State University
University Park, PA

[2]Applied Research Lab
The Pennsylvania State University
University Park, PA

[3]Electrical Engineering
The Pennsylvania State University
University Park, PA

## ABSTRACT

*There are over three million wheelchair users within the United States and that number is growing. This paper is concerned with improving the safety of wheelchair operation by the on-line estimation of tire slip. Wheelchair tire slip is a result of icy or low friction surfaces, often representative of dangerous conditions. In this research, wheel slip is detected by estimating the instantaneous center of rotation (ICR) locations of wheelchair wheels relative to the ground surface. Any departure of the estimated ICR positions from the wheel contact point indicates slippage is occurring.*

*An Extended Kalman Filter (EKF) algorithm uses inputs of position and orientation obtained via map-based localization to detect changes in wheelchair ICR location estimates. The ICR EKF algorithm is verified in simulation. A robotic wheelchair is used for testing the presented algorithms under conditions inducing tire slip. The results show that the ICR locations do not vary significantly when the wheelchair is operated under normal conditions, i.e. low slip surfaces; however, they change significantly under slip conditions. Implementing this method with electric wheelchairs can improve the prediction of wheelchair motion on slippery surfaces, enabling warning systems and safe operational modes that can enhance the safety of wheelchair users.*

## 1 INTRODUCTION

There are approximately 3.6 million wheelchair users in the United States [1]. As the U.S. population ages, health care opportunities advance, and mobility device design progresses, the use and importance of these assistive devices will increase [2]. In particular, the safety of these devices in a broad range of environments must be ensured.

Winter and rainy weather conditions present added difficulty for people who use wheelchairs, often putting further constraints on mobility [3–5]. Many people elect to remain home rather than risk driving their wheelchairs outside in a potentially unsafe environment caused by winter precipitation [3]. As Lemaire, *et al.*, note, this inhibition can contribute to social isolation, as well as psychosocial problems. Much of this problem is a result of drive and caster wheels slipping on snow and ice [3,6]. However, there has been very little research attributed to improving the control of wheelchair motion on slippery terrains [3,7].

The aim of this work is to implement an algorithm used by Pentzer, *et al.*, to better predict the motion of wheelchairs on slippery surfaces, as well as assist in accounting for wheelchair motion inclusive of caster wheels in real-time [8,9]. Caster wheels are almost always included in wheelchair design for stability; however, they can decrease the accuracy of a two-wheel differential drive kinematic model. While kinematic models including caster wheels do exist, they are extremely difficult to implement with the motion model and are often neglected.

The algorithm developed by Pentzer, *et al.*, estimates the location of track instantaneous centers of rotation (ICRs) on a skid-steer mobile robot [8, 9]. Similar to differential-drive vehicles, skid-steer robotics adjust right and left track speeds to produce rotational motion. However, skid-steer vehicles rely on track slippage for turning maneuvers. As stated by Pentzer, *et al.*,

*Address all correspondence to klw372@psu.edu.


Copyright © 2016 by ASME

ICR kinematics for both skid-steer robots and differential drive robots can provide accurate open-loop motion estimates when operated at low speeds on flat, hard terrain [8–10]. Additionally, ICR locations can be accurately estimated during robot operation using an Extended Kalman Filter (EKF), after which the required wheel or track speeds for a desired vehicle movement may be calculated [8, 9]. The ICR locations estimated via the EKF provided a mapping from the vehicle wheel or track speeds to vehicle forward and angular velocity. This method has been proposed to aid in model-based motion prediction of skid-steer robots and improve the accuracy of odometry in the absence of global positioning system (GPS) measurements.

The purpose of this paper is to improve the safety of wheelchair operation via the on-line estimation of tire slip. The remainder of this work is organized as follows: Section 2 outlines the ICR kinematics and the EKF developed to estimate the ICR locations; in Section 3, the simulation and simulated results for algorithm verification are presented; Section 4 introduces the design of the robotic wheelchair platform used for testing, as well as the methods used for experimentation; Section 5 describes the experimental results obtained; finally, in Section 6, the contributions of this work and future work are discussed.

## 2 METHODOLOGY

This section outlines the ICR kinematics equations and the EKF algorithm developed in [8,9] to estimate the ICR locations. In Section 2.1, the calculations to obtain the lateral and longitudinal ICR locations for the wheelchair's right wheel, left wheel, and chassis, as well as the wheelchair's longitudinal, lateral, and angular velocities are presented. The kinematic motion model and measurement equations used for the EKF algorithm are given in Section 2.2.

### 2.1 ICR Kinematics

The typical kinematic equations for two-wheeled robots make several major assumptions; the equations assume the robot is traveling over flat terrain, with no tire deformation, and that no slipping occurs at the contact point between the drive wheels and the ground surface [11]. Unfortunately, these simplifying assumptions are not indicative of real-world operating conditions. Rather, road and sidewalk surfaces are not always flat and wheels deform under different loads. These deviations in behavior can be measured from sensory inputs, especially when slipping occurs, such as in poor weather conditions.

This work applies the ICR kinematics developed by [8–10, 12] to a robotic wheelchair system to enhance the prediction of the wheelchair's motion when the typical kinematic assumptions fail. The ICR locations relative to the wheelchair with positive $X$ in the forward direction, positive $Y$ to the right, and positive $Z$ down are shown in Fig. 1. The lateral ICR location between

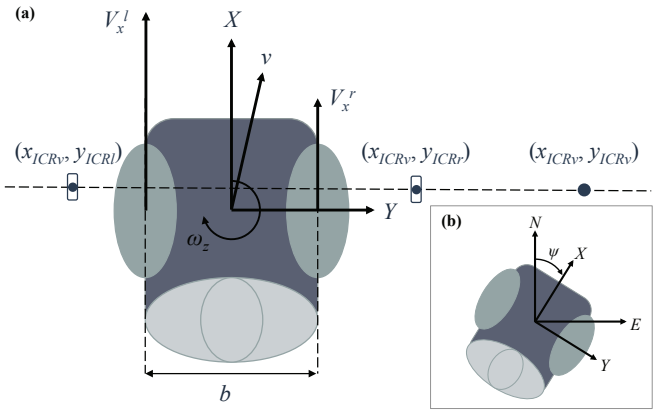


**FIGURE 1**. A diagram of the ICR locations for the robotic wheelchair when undergoing slippage.

the wheelchair body and the ground, $y_{ICRv}$, is a point along the $Y$-axis for which there is zero instantaneous velocity. The lateral ICR location is given by

$$y_{ICRv} = \frac{v_x}{\omega_z} \tag{1}$$

where $v_x$ and $\omega_z$ are the longitudinal and angular velocities of the wheelchair, respectively. The ICR locations between the right and left tires and the ground, $y_{ICRl}$ and $y_{ICRr}$, are

$$y_{ICRl} = -\frac{V_x^l - v_x}{\omega_z} \tag{2}$$

$$y_{ICRr} = -\frac{V_x^r - v_x}{\omega_z} \tag{3}$$

where $V_x^l$ and $V_x^r$ are the velocities of the left and right tires relative to the body of the wheelchair, respectively. The longitudinal ICR location between the tires and the ground, $x_{ICRv}$, is given by

$$x_{ICRv} = -\frac{v_y}{\omega_z} \tag{4}$$

where $v_y$ is the lateral velocity of the wheelchair. The longitudinal ICR locations between the left and right tires and the ground, $x_{ICRl}$ and $x_{ICRr}$, can be computed similarly to Eqn. (2) and Eqn. (3),


Copyright © 2016 by ASME

$$x_{ICRl} = \frac{V_y^l - v_y}{\omega_z} \tag{5}$$

$$x_{ICRr} = \frac{V_y^r - v_y}{\omega_z} \tag{6}$$

However, since the wheelchair tires are nonholomonically constrained, the velocity in the $Y$ direction is assumed to be zero, simplifying Eqn. (5) and Eqn. (6) to

$$x_{ICRr} = x_{ICRl} = x_{ICRv} = -\frac{v_y}{\omega_z} \tag{7}$$

As noted in [9], the values of the lateral ICR locations, $y_{ICRv}$, range within $\pm\infty$ depending upon the motion of the wheelchair. Conversely, the ICR locations $y_{ICRr}$, $y_{ICRl}$, and $x_{ICRv}$ remain bounded [10].

Equations (2)-(4) can then be solved simultaneously for the wheelchair's longitudinal, lateral, and angular velocities, $v_x$, $v_y$, and $\omega_z$, respectively, as a function of left and right wheel speeds, $V^l$ and $V^r$.

$$v_x = \frac{V_x^r y_{ICRr} - V_x^l y_{ICRl}}{y_{ICRl} - y_{ICRr}} \tag{8}$$

$$v_y = \frac{(V_x^l - V_x^r) x_{ICRv}}{y_{ICRl} - y_{ICRr}} \tag{9}$$

$$w_z = -\frac{V_x^l - V_x^r}{y_{ICRl} - y_{ICRr}} \tag{10}$$

The EKF discussed in Section 2.2 is founded upon Eqs. (8)-(10) in order to predict the ICR locations.

## 2.2 EKF Estimation of ICR Locations

The EKF in this section has been derived in [9] to identify the ICR locations of tracked and wheeled skid-steer vehicles using inputs of track and wheel speeds as well as vehicle position and heading. A flow diagram outlining how sensor data is input into the EKF is illustrated in Fig. 2. Individual wheel velocities are obtained from odometry data while the wheelchair's position and orientation are supplied by a map-based localization algorithm. The wheel velocities, as well as the wheelchair position and orientation are input into the EKF which then yields improved estimates for wheelchair position, orientation, and ICR locations.

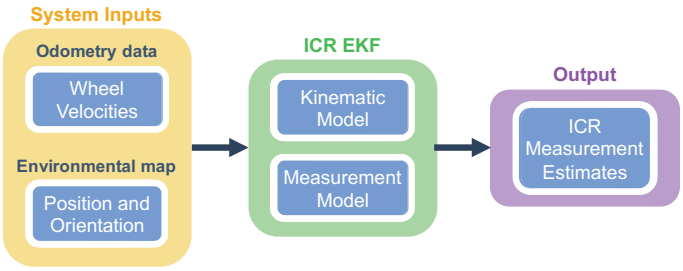


**FIGURE 2**. Flow diagram outlining the EKF algorithm system inputs and outputs.

A fixed north-east-down (NED) frame with a positive clockwise heading angle $\psi$, shown in Fig. 1, will be used as the wheelchair's frame of reference throughout this work. The wheelchair velocities can be found from Eqs. (8)-(10)

$$\dot{N} = v_x \sin(\psi) + v_y \cos(\psi) \tag{11}$$

$$\dot{E} = v_x \cos(\psi) - v_y \sin(\psi) \tag{12}$$

Augmenting Eqs. (10), (11), and (12) and assuming ICR locations remain constant results in the following continuous-time kinematic motion model:

$$\begin{bmatrix} \dot{N} \\ \dot{E} \\ \dot{\psi}_z \\ \dot{y}_{ICRr} \\ \dot{y}_{ICRl} \\ \dot{x}_{ICRv} \end{bmatrix} = \begin{bmatrix} v_x \sin(\psi) + v_y \cos(\psi) + \omega_N \\ v_x \cos(\psi) - v_y \sin(\psi) + \omega_E \\ -\frac{V_x^l - V_x^r}{y_{ICRl} - y_{ICRr}} + \omega_\omega \\ \omega_r \\ \omega_l \\ \omega_x \end{bmatrix} \tag{13}$$

Discretizing Eqn. (13) we obtain the discrete-time kinematic


Copyright © 2016 by ASME

motion model:

$$\begin{bmatrix} N_k \\ E_k \\ \psi_k \\ y_{ICRr_k} \\ y_{ICRl_k} \\ x_{ICRv_k} \end{bmatrix} = \begin{bmatrix} N_{k-1} + \Delta t V_{N_{k-1}} + \Delta t\, \omega_N \\ E_{k-1} + \Delta t V_{E_{k-1}} + \Delta t\, \omega_E \\ \psi_{k-1} + \Delta t\, \omega_{z_{k-1}} + \Delta t\, \omega_\omega \\ y_{ICRr_{k-1}} + \Delta t\, \omega_r \\ y_{ICRl_{k-1}} + \Delta t\, \omega_l \\ x_{ICRv_{k-1}} + \Delta t\, \omega_x \end{bmatrix} \tag{14}$$

where $\Delta t$ is the time step and $\omega_E$, $\omega_N$, $\omega_\omega$, $\omega_r$, $\omega_l$, and $\omega_x$ are additive zero-mean Gaussian process noises. For vehicles traveling at low speeds on hard, flat terrain, which is the most common case for wheelchairs, ICR locations have previously been shown to remain within a small bounded regain [9, 10]. Consequently, the ICR locations can be modeled as constants disturbed by random noise.

Measurements of the wheelchair's position, $N$, $E$, and orientation, $\psi$ are used to update the EKF's state measurement vector, $\mathbf{y}$, given by Eqn. (15).

$$\mathbf{y}_k = \begin{bmatrix} N_k \\ E_k \\ \psi_k \end{bmatrix} \tag{15}$$

.
The measurement equations are then obtained as follows:

$$\mathbf{h}_k = \begin{bmatrix} N + v_N \\ E + v_E \\ \psi + v_\psi \end{bmatrix}, \tag{16}$$

where $v_N$, $v_E$, and $v_\psi$ represent additive measurement noise. The standard EKF equations can then be implemented as in [9].

## 3 SIMULATION AND ANALYSIS OF ICR EKF

For the initial validation of the ICR EKF algorithm, a two-dimensional simulation is implemented modeling the true wheelchair's motion using the kinematic motion model in Eqn. (14). The ICR locations are initialized to lie directly beneath the wheelchair's wheels, such that $y_{ICRr} = 0.254$ m, $y_{ICRl} = -0.254$ m, and $x_{ICRv} = 0.0$ m. The path of the wheelchair is varied by adding zero-mean Gaussian noise to the left and right wheel velocity inputs, as well as by the measurement and process noise parameters. Wheelchair tire slip is simulated by adding additional noise to the right or left wheel velocity inputs at various time periods.

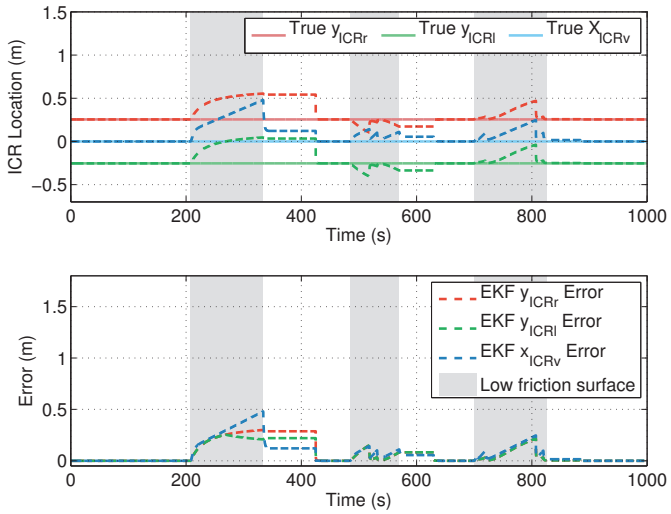


**FIGURE 3**. The simulated ICR estimates undergo little variation when the simulation undergoes low slip; however, they change significantly when simulated slip is induced.

### 3.1 Simulation Results

The results show that the ICR locations do not vary significantly under normal simulated conditions, i.e. low slip surfaces; however, they change significantly under simulated slip conditions, as observed in Fig. 3. Consequently, the EKF is able to accurately predict the orientation and position of the wheelchair. A comparison of the simulated wheelchair's true heading to that of the EKF's predicted heading is shown in Fig. 4, in which negligible error is seen between the two heading values. The simulated wheelchair's true and estimated positions have no discrepancies and are shown in Fig. 5. The convergence time of the filter depends heavily on the motion of the wheelchair. If the wheelchair is driven perfectly straight, the ICR estimates will not be updated. Rather, the ICR locations are learned while the angular rate is nonzero, which occurs when the wheelchair turns.

## 4 EXPERIMENTATION

A Jazzy Pride Select 6 (Pride Mobility Products Corp., USA) was used to gather experimental testing data and is shown in Fig. 6. The wheelchair has been modified with a variety of sensors. Wheelchair position and orientation measurements are obtained from an open-source adaptive Monte-Carlo map-based localization package using a Hokuyo URG-04LX scanning laser rangefinder. The wheel velocities were obtained via HB6M Hollow Bore Optical Encoders (US Digital, USA). For comparison between the ICR EKF algorithm and odometry-based predictions over low-friction surfaces, the wheelchair position and orientation were also analyzed from measurements provided by the encoders and compared to the map-based localization estimates.


Copyright © 2016 by ASME

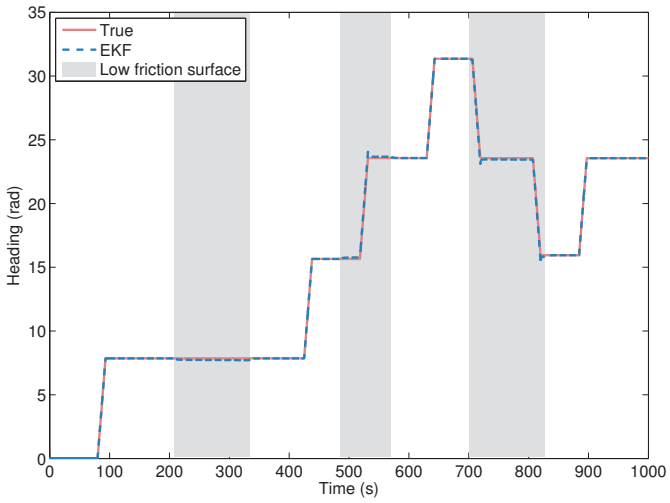


**FIGURE 4**. Comparison of simulated true and predicted wheelchair heading. There is negligible error between the two heading values.

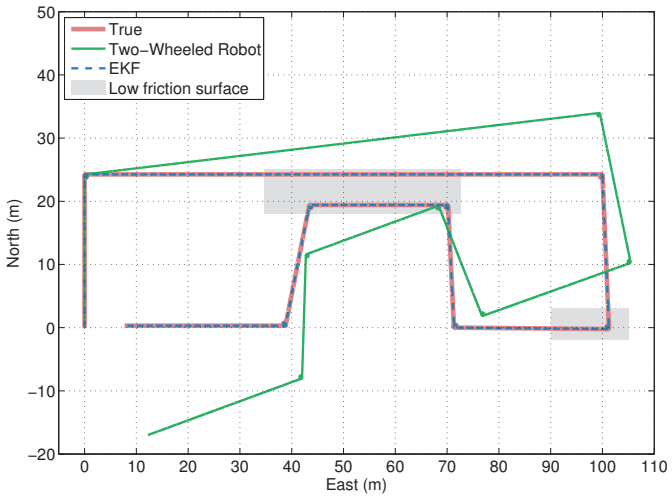


**FIGURE 5**. The simulated wheelchair's true and estimated positions with low friction surfaces shown in grey.

To validate the ICR EKF algorithm experimentally, the wheelchair was driven first on a non-slip inducing surface to allow the ICR location estimates to converge to their true locations. Once converged, the wheelchair was driven over a low friction surface to induce slip on the tires. The experimental results are presented in the following section.

## 5 RESULTS

As predicted in the simulated results, it is experimentally observed that the ICR locations do not vary significantly when the wheelchair is operated under low slip surface conditions, as

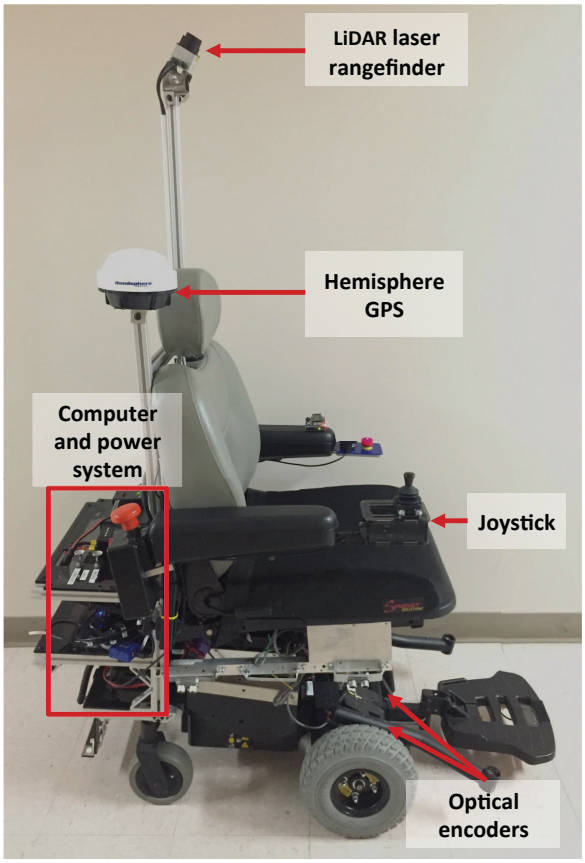


**FIGURE 6**. An image of the robotic wheelchair used for experimentation. Measurements of position and orientation are obtained via map-based localization and measurements of individual wheel velocities are obtained from odometry.

shown in Fig. 7. The algorithm most quickly converges when the EKF is initialized with the previous ICR estimates, resulting in minimal variations in the ICR locations. The ICR locations will then only change significantly when the wheelchair tires are undergoing slip. If the EKF is initialized with poor ICR estimates, the algorithm will take longer to converge on the actual ICR locations. The convergence time of the algorithm is also dependent upon the motion of the wheelchair, as mentioned in Section 3, and a nonzero angular rate is necessary for the algorithm to learn the ICR locations. Furthermore, it can be observed that the ICR locations do remain bounded to the same region under normal operating conditions and low-friction conditions, as discussed in Section 2.2.

The ICR errors between the measured and true locations are shown in Fig. 8. It is observed that the ICR estimates undergo a brief increase in error prior to converging, but then quickly converge to very near their true states. Interestingly, it is the error observed in the ICR states after convergence that lends the most


Copyright © 2016 by ASME

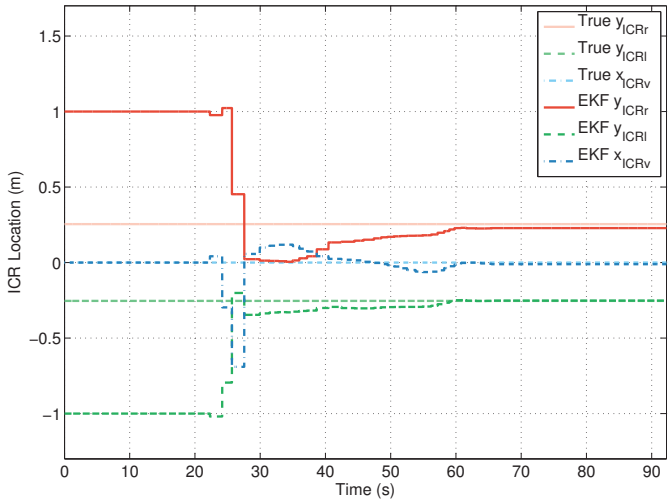


**FIGURE 7**. The experimentally collected ICR estimates take some time to converge; however, once converged, they change significantly little even when slip is induced.

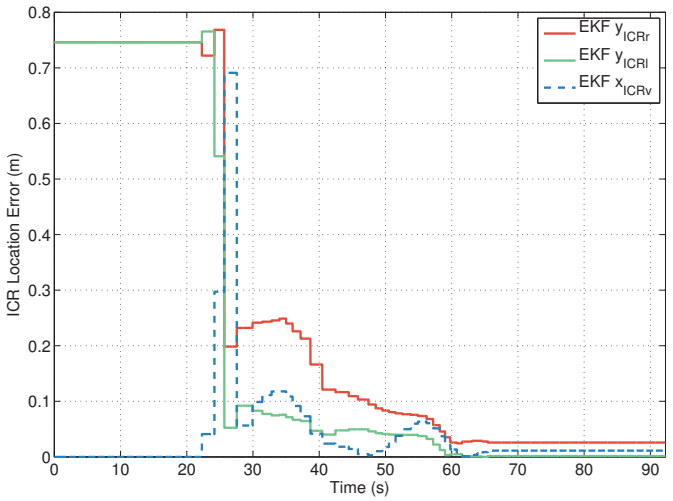


**FIGURE 8**. The errors observed in the experimentally collected ICR estimates. The largest errors occur as the ICR estimates converge. Once converged, the errors are negligible

benefit to the safety of the wheelchair system. When the ICR error is negligible, it can be safely assumed that the wheelchair is not undergoing significant slippage. However, the changing ICR locations and subsequent errors indicative of slip can then be utilized to enhance wheelchair safety. When error is present between the true and actual ICR values, the wheelchair system can enter a slip-safe operational mode. A number of slip-safe operational modes are possible, ranging from simply limiting the top speed, to implementing an anti-skid system onboard the wheelchair, analogous to anti-lock brakes on passenger vehicles.

The improved accuracy of the EKF to estimate the wheelchair's heading and position can be seen in Fig. 9. The point at which the ICR locations begin to converge are observed as an offset in the EKF's predicted wheelchair position in comparison to the map-based localization algorithm's more accurate estimate of the wheelchair's position. As the wheelchair traverses over the low friction surface, the ICR locations have converged to approximately their true locations; consequently, the EKF algorithm estimates the position of the wheelchair within an error of 0.36 meters in the x-direction and 0.50 meters in the y-direction. Conversely, maximum odometry measurement errors are 0.64 meters in the x-direction and 0.88 meters in the y-direction, as shown in Fig. 10. While the implementation of the ICR EKF algorithm yields a significant improvement in the position estimate of the wheelchair, the result is still not accurate enough to be relied upon as the only method of wheelchair localization. The position estimate of the ICR EKF position estimates could be improved with the implementation of a more accurate localization method.

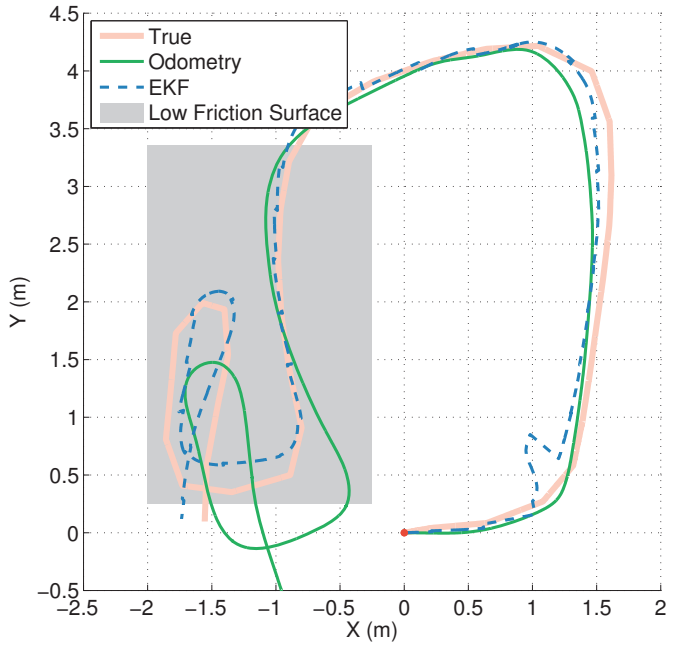


**FIGURE 9**. Comparison of the wheelchair's true position (as provided by map-based localization), odometry-based position measurement, and the EKF estimated position with the low friction surface shown in grey.

## 6 CONCLUSIONS AND FUTURE WORK

Wheelchair tire slip is a result of icy or low friction surfaces, often representative of dangerous conditions. This research aims to detect wheel slip by estimating the ICR locations


Copyright © 2016 by ASME

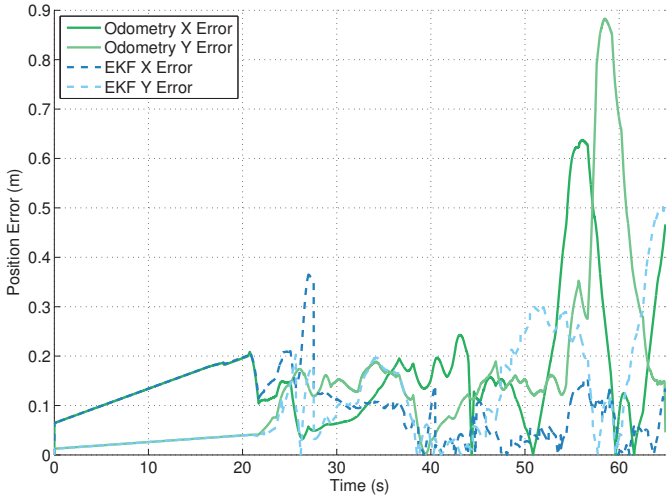


**FIGURE 10**. Comparison of $x$ and $y$ position errors between the wheelchair's true position (as provided by map-based localization) and odometry measurements, as well as the wheelchair's true position and the EKF estimates.

of wheelchair wheels relative to the ground surface in order to enhance the safety of wheelchair users. The results show that the ICR locations do not vary significantly when the wheelchair is operated under normal conditions, i.e. low slip surfaces; however, they change significantly under low friction conditions. This result is significant because the changing ICR values indicative of slip can be utilized to enable warning systems and slip-safe operational modes. In addition, a significant problem with odometry-based navigation is the error accumulation over long distances due to drift, which affects measurements of both the wheelchair's position and orientation, particularly on surfaces with low friction. By utilizing ICR EKF estimates, the position and orientation of the wheelchair can also be better predicted. The implementation of this technique with electric powered wheelchairs can improve the prediction of wheelchair motion on slippery surfaces, thus enabling warning systems and safe operational modes that can enhance the safety of wheelchair users. Future work includes improving the ICR EKF location estimates via the implementation of a more accurate localization method.

## ACKNOWLEDGMENT

This material is based upon work supported by the National Science Foundation under Grant No. DGE1255832. Any opinions, findings, and conclusions or recommendations expressed in this material are those of the author(s) and do not necessarily reflect the views of the National Science Foundation.

## REFERENCES

[1] Brault, M. W., of the Census, U. S. B., et al., 2012. *Americans with disabilities: 2010*. US Department of Commerce, Economics and Statistics Administration, US Census Bureau.

[2] Kaye, H. S., Kang, T., and LaPlante, M. P., 2000. *Mobility device use in the United States*, Vol. 14. National Institute on Disability and Rehabilitation Research, US Department of Education.

[3] Lemaire, E. D., O'Neill, P. A., Desrosiers, M. M., and Robertson, D. G., 2010. "Wheelchair ramp navigation in snow and ice-grit conditions". *Archives of physical medicine and rehabilitation,* ***91***(10), pp. 1516–1523.

[4] Gao, C., and Abeysekera, J., 2004. "Slips and falls on ice and snow in relation to experience in winter climate and winter sport". *Safety science,* ***42***(6), pp. 537–545.

[5] Bentley, T. A., 1998. "Slip, trip and fall accidents occurring during the delivery of mail". *Ergonomics,* ***41***(12), pp. 1859–1872.

[6] Shirado, O., Shundo, M., Kaneda, K., and Strax, T. E., 1995. "Outdoor winter activities of spinal cord-injured patients: With special reference to outdoor mobility.". *American journal of physical medicine & rehabilitation,* ***74***(6), pp. 408–414.

[7] Rousseau, J., Aissaoui, R., and Bourbonnais, D., 2005. "Measuring the effort needed to climb access ramps in a manual wheelchair". *CMHC-SCHL Research Highlight*, pp. 1–4.

[8] Pentzer, J., Brennan, S., and Reichard, K., 2014. "The use of unicycle robot control strategies for skid-steer robots through the icr kinematic mapping". In Intelligent Robots and Systems (IROS 2014), 2014 IEEE/RSJ International Conference on, IEEE, pp. 3201–3206.

[9] Pentzer, J., Brennan, S., and Reichard, K., 2014. "Model-based prediction of skid-steer robot kinematics using online estimation of track instantaneous centers of rotation". *Journal of Field Robotics,* ***31***(3), pp. 455–476.

[10] Martínez, J. L., Mandow, A., Morales, J., Pedraza, S., and García-Cerezo, A., 2005. "Approximating kinematics for tracked mobile robots". *The International Journal of Robotics Research,* ***24***(10), pp. 867–878.

[11] Kelly, A., and Seegmiller, N., 2014. "A vector algebra formulation of mobile robot velocity kinematics". In Field and Service Robotics, Springer, pp. 613–627.

[12] Mandow, A., Martinez, J. L., Morales, J., Blanco, J. L., Garcia-Cerezo, A., and Gonzalez, J., 2007. "Experimental kinematics for wheeled skid-steer mobile robots". In Intelligent Robots and Systems, 2007. IROS 2007. IEEE/RSJ International Conference on, IEEE, pp. 1222–1227.



Copyright © 2016 by ASME